UNIVERSITY *of York*

This is a repository copy of *Pyrophosphate release acts as a kinetic checkpoint during high-fidelity DNA replication by the Staphylococcus aureus replicative polymerase PolC*.

White Rose Research Online URL for this paper:
https://eprints.whiterose.ac.uk/217626/

Version: Published Version

Article:

Fagan, Sean P, Mukherjee, Purba orcid.org/0000-0001-9869-6509, Jaremko, William J et al. (6 more authors) (2021) Pyrophosphate release acts as a kinetic checkpoint during high-fidelity DNA replication by the Staphylococcus aureus replicative polymerase PolC. Nucleic Acids Research. pp. 8324-8338. ISSN 0305-1048

White Rose
university consortium
Universities of Leeds, Sheffield & York

eprints@whiterose.ac.uk
https://eprints.whiterose.ac.uk/

Pyrophosphate release acts as a kinetic checkpoint during high-fidelity DNA replication by the *Staphylococcus aureus* replicative polymerase PolC

Sean P. Fagan[1,2], Purba Mukherjee[1,2], William J. Jaremko[1], Rachel Nelson-Rigg[1,2], Ryan C. Wilson[1], Tyler L. Dangerfield[3], Kenneth A. Johnson[3], Indrajit Lahiri[1,2,4,*] and Janice D. Pata [ORCID][1,2,*]

[1]Wadsworth Center, New York State Department of Health, Albany, NY, USA, [2]Department of Biomedical Sciences, University at Albany, Albany, NY, USA, [3]Institute for Cellular and Molecular Biology, The University of Texas at Austin, Austin, TX, USA and [4]Department of Biological Sciences, Indian Institute of Science Education and Research, Mohali, Punjab, India

ABSTRACT

Bacterial replication is a fast and accurate process, with the bulk of genome duplication being catalyzed by the α subunit of DNA polymerase III within the bacterial replisome. Structural and biochemical studies have elucidated the overall properties of these polymerases, including how they interact with other components of the replisome, but have only begun to define the enzymatic mechanism of nucleotide incorporation. Using transient-state methods, we have determined the kinetic mechanism of accurate replication by PolC, the replicative polymerase from the Gram-positive pathogen *Staphylococcus aureus.* Remarkably, PolC can recognize the presence of the next correct nucleotide prior to completing the addition of the current nucleotide. By modulating the rate of pyrophosphate byproduct release, PolC can tune the speed of DNA synthesis in response to the concentration of the next incoming nucleotide. The kinetic mechanism described here would allow PolC to perform high fidelity replication in response to diverse cellular environments.

INTRODUCTION

DNA polymerases catalyze the fundamental process of genome duplication. To ensure the integrity of the genetic information, multiple DNA polymerases are required, each with a specific role in DNA replication, repair, and damage tolerance ([1]). Biochemical and structural studies over the past four decades have shown that all DNA polymerases share the same two-metal-ion catalytic mechanism for deoxynucleoside triphosphate (dNTP) addition (Figure 1A) ([2,3]). Yet differences in substrate specificity and nucleotide incorporation fidelity, defined by the kinetics of individual steps in the reaction pathway (Figure 1B) ([4–7]), confer distinguishing characteristics that allow different polymerases to perform their unique functions ([8]).

Early kinetic characterization of the A-family polymerases *Escherichia coli* DNA polymerase I and T7 DNA polymerase established a common minimal kinetic model for nucleotide incorporation by DNA polymerases (Figure 1B) ([9–11]). First, polymerase binds DNA to form a binary complex (Pol•DNA$_n$). Second, the Pol•DNA$_n$ complex binds a nucleotide to form the pre-chemistry ternary complex (Pol•DNA$_n$•dNTP). The chemical step of bond formation is often preceded by conformational changes in the Pol•DNA$_n$•dNTP complex allowing the dNTP to transition from ground state binding to the active state, competent for catalysis ([6,7]). The bound nucleotide is then incorporated rapidly into the primer strand to form a post-chemistry ternary complex with bound pyrophosphate (PP$_i$) byproduct (Pol•DNA$_{n+1}$•PP$_i$). The chemistry of nucleotide incorporation is facilitated by two universally conserved aspartate residues that coordinate two divalent metal cations (Figure 1A) ([2,3]). Following chemistry, PP$_i$ is then rapidly released, thus completing the addition of the deoxynucleoside monophosphate (dNMP) to the DNA substrate. At this stage there are two possibilities: for distributive synthesis, the polymerase dissociates from the extended DNA (DNA$_{n+1}$), while for processive synthesis the poly-
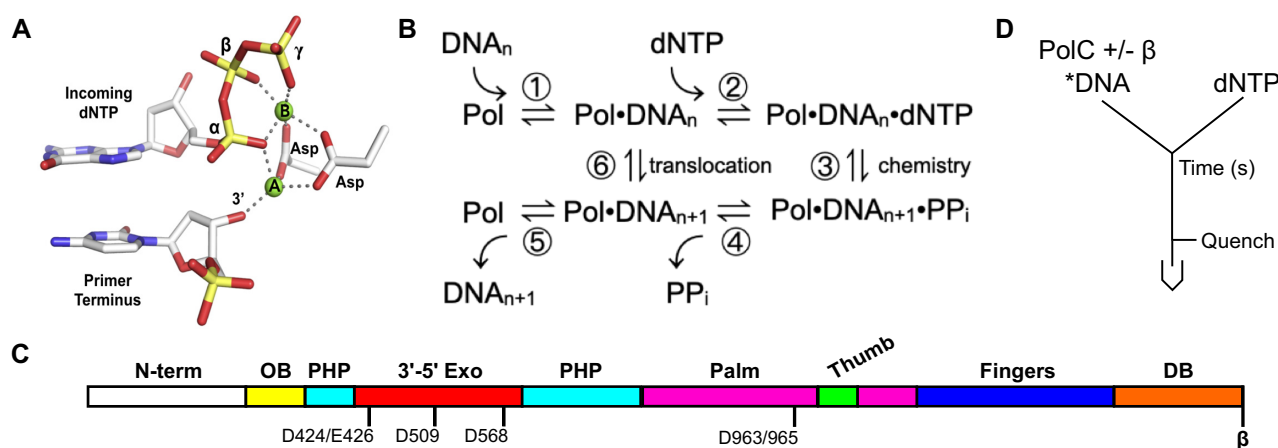
Figure 1. Polymerase catalytic mechanism, PolC domain organization and reaction scheme for kinetic measurements. (**A**) Two-metal-ion mechanism utilized by DNA polymerases to catalyze the nucleotidyl transfer reaction. Divalent metal ions A and B which facilitate the reaction are coordinated by two universally conserved aspartates. (**B**) Minimal kinetic pathway for nucleotide addition by a DNA polymerase (Pol). (**C**) Domain architecture of PolC with the catalytic residues for both the polymerase and proofreading exonuclease activities of *S. aureus* PolC indicated. OB: oligonucleotide binding domain (yellow); PHP: polymerase and histidinol phosphatase domain (cyan); DB: duplex binding domain (orange); β: clamp binding motif. The palm (magenta), thumb (green), fingers (blue) and DB domains form the polymerase region that defines the C-family polymerases. (**D**) Generalized reaction set-up for the kinetic characterization of PolC using rapid quench-flow methods. (*) FAM label.

merase translocates along the DNA and the catalytic cycle is repeated for the addition of all subsequent nucleotides. Fidelity of nucleotide incorporation by high-fidelity DNA polymerases is ensured by several mechanisms. At the structural level, the polymerase active site imposes steric constraints for proper Watson-Crick base pairing and the selection of deoxynucleotides over ribonucleotides (12–14). Free-energy differences in the kinetic pathway caused by the alignment of active site residues distinguish between correct and incorrectly paired bases to ensure incorporation of proper Watson–Crick base pairs (4,5). Additionally, nucleotide-induced conformational changes select correct nucleotides for incorporation while promoting release of mismatched nucleotides (6,7). Finally, the association of proofreading subunits or presence of intrinsic proofreading domains increase polymerase fidelity by two- to three-orders of magnitude (12,15).

Although the bacterial replisome has served as a paradigm for understanding the machinery required for DNA replication, structure-function studies of the polymerases at the core of the replisome have lagged far behind those of other polymerase families, but that is slowly changing. Several structures of bacterial replicative DNA polymerases, the α subunit of DNA polymerase III (Pol IIIα), have now been reported. These include apo-enzyme, binary, and ternary complex structures of DnaE from the Gram-negative bacteria *E. coli* and *Thermus aquaticus*, and from *Mycobacterium tuberculosis*, as well as the ternary complex structure of PolC from the Gram-positive bacterium *Geobacillus kaustophilus* (16–21). These C-family polymerases share the same polymerase catalytic core, comprised of palm, thumb, fingers and duplex binding domains (Figure 1C), but the PolC and DnaE branches differ in domain organization outside of these regions. Strikingly, as revealed from structural comparisons of the catalytic domains, the bacterial and eukaryotic replicative polymerases do not share a common ancestor but have undergone con-

vergent evolution to perform the same cellular function (22,23). In fact, the bacterial replicative polymerases are distantly related to X-family polymerases such as human DNA polymerase β (24), which is involved in base-excision repair (16,18,20).

Here, we report the kinetic mechanism of DNA replication by PolC, the replicative DNA polymerase from the Gram-positive pathogen *Staphylococcus aureus*. Together with our previous work on a truncated version of the same enzyme (25), this study provides the first comprehensive overview of the kinetics of DNA synthesis by a C-family polymerase. Our results reveal a unique mechanism employed by PolC to ensure fast and accurate DNA synthesis. We found that the release of PP_i following the addition of a dNTP acts as a catalytic checkpoint for PolC. In the presence of the next correct incoming nucleotide, PP_i release is fast, allowing rapid DNA synthesis. However, if the next correct dNTP is not present then PP_i release becomes rate-limiting, slowing the processive synthesis cycle. To our knowledge this is the first report of a kinetic mechanism that allows a DNA-dependent DNA polymerase to ensure the presence of the next correct nucleotide before committing to completion of the current nucleotide addition cycle.

MATERIALS AND METHODS

Cloning of *S. aureus* PolC Exo^Mut and β-clamp

The *polC* gene from *S. aureus* strain COL was synthesized and codon-usage was optimized for expression in *E. coli* by GenScript, Corp. (NJ, USA). The *polC* gene was cloned into pET28a (+) using restriction sites NcoI and BamHI, with an N-terminal deca-histidine tag followed by a TEV cleavage site. Residues in the exonuclease active site at positions D424, E426, D509 and D568 were mutated to alanine to prevent degradation of nucleic acids. This mutated construct of *S. aureus* PolC will be referred to as PolC. The *S. aureus dnaN* gene which codes for the β-clamp along with

a C-terminal hexa-histidine tag, cloned into pET23a was a gift from Dr. Michael O'Donnell, The Rockefeller University (26).

Expression and purification of PolC and β-clamp

To express PolC, the plasmid was transformed into Rosetta (DE3) pLysS cells. Cultures were grown at 37°C to an OD_{600} of ~0.6 and induced by addition of 0.5 mM IPTG for ~18 h at 17°C before harvesting by centrifugation. Purification was performed as described previously (25). Fractions containing PolC were concentrated using Amicon centrifugal filters (Millipore-Sigma) (50 kDa MWCO) and quantified by measuring the absorbance at 280 nm (A_{280}) using the theoretical extinction coefficient of 113 000 $M^{-1} cm^{-1}$. PolC aliquots were flash frozen in liquid nitrogen and stored at –80°C.

To express β-clamp, the plasmid encoding *dnaN* was transformed into Rosetta (DE3) pLysS cells. Cultures were grown at 37°C to an OD_{600} of ~0.6 and induced by addition of 0.5 mM IPTG for ~18 h at 17°C before harvesting by centrifugation. Purification was performed at 4°C as follows. Cell pellets were re-suspended in lysis buffer (25 mM HEPES pH 7.5, 1 M NaCl, 50 mM imidazole, and 10% [v/v] glycerol), lysed by sonication and clarified by centrifugation. The clarified cell lysate was loaded on HisTrap HP (GE Life Sciences) (2 × 5 ml) columns charged with Ni^{2+} and washed with lysis buffer. Protein was eluted with Ni buffer B (25 mM HEPES 7.5, 500 mM NaCl, 1 M imidazole and 10% [v/v] glycerol) using a linear gradient from 50 mM to 1 M imidazole. For all purification steps, fractions were analyzed using 4–20% SDS-PAGE. Fractions containing the clamp were pooled and diluted to 250 mM NaCl for loading onto HiTrap Q HP (GE Life Sciences) (2 × 5 ml) columns and washed with Q buffer A (25 mM HEPES 7.5, 250 mM NaCl, 0.1 mM EDTA, 10% [v/v] glycerol and 5 mM DTT). Protein was eluted over a linear gradient from 250 mM to 1 M NaCl in Q buffer B (25 mM HEPES pH 7.5, 1 M NaCl, 0.1 mM EDTA, 10% [v/v] glycerol and 5 mM DTT). Fractions containing clamp were pooled and loaded onto a Superdex 75 PG 26/60 column (GE Life Sciences) equilibrated with Q buffer A. Fractions containing the clamp were concentrated using Amicon centrifugal filters (Millipore-Sigma) (30kDa MWCO) and quantified by A_{280} using the theoretical extinction coefficient of 15 930 $M^{-1} cm^{-1}$ (from the amino acid sequence of a single monomer). Aliquots of β-clamp were flash frozen in liquid nitrogen and stored at –80°C.

DNA substrates

Synthetic DNA oligonucleotides, either labeled at the 5′ end with 6-FAM or unlabeled, were purchased from Integrated DNA Technologies, Inc. Primer 1 (5′-CCCATCGTATACTCGAATCT GTCCTGTGTG-3′) or primer 2 (5′-CCCATCGTATACTCGAAT CTGTCCTGTGTGT-3′) were annealed to template 1 (5′- CATGCAAGCTTGGCACTGCGAAAC GGAGACAGCAGGTACACACAGGACAGATTC GAGTATACGATGGG-3′) to form substrate S1 or S2, respectively. Primer 3 (5′-TCGAATCTGTCCTGTGT

G-3′) was annealed to template 2 (5′-GAAACGGAGACA GCAGGTACACACAGGACAGATTCGA-3′) to form substrate S3. Annealing reactions were performed with a 1:1.1 ratio of primer to template oligonucleotide strands, in 10 mM Tris–Cl pH 8.0 and 50 mM NaCl by denaturing at 95°C and gradually cooling to room temperature.

DNA extension assays with a single nucleotide

All quench-flow assays were performed on a KinTek Corp. (Austin, TX, USA) RQF-3 rapid quench instrument at 25°C in PolC reaction buffer (25 mM MES–Tris pH 7.5, 25 mM NaCl, 8 mM $MgCl_2$, 2 mM DTT, 0.5 μM BSA and 5% [v/v] glycerol). All reactions, unless mentioned otherwise, contain a premix of 1 μM PolC (220 nM active PolC) and 40 μM β monomer (20 μM β-clamp). Reactions were quenched with quench buffer (250 mM EDTA and 50% [v/v] formamide) and analyzed using a denaturing 17% polyacrylamide (19:1) gel containing 7M Urea and 1X TBE run at 55°C. All gels were imaged on a Typhoon RGB (GE Life Sciences) scanner with an excitation wavelength of 488 nm (blue laser) and an emission cutoff of 525 nm. Products were quantitated as the fraction of extended primer relative to the total primer (extended and un-extended). To determine binding affinity of PolC for DNA with or without clamp, DNA extension assays were performed by mixing equal volumes of PolC, β-clamp monomer (in case of with clamp) and DNA substrate S3 (0.1, 0.2, 0.4, 0.8 and 1.6 μM, without clamp) or DNA substrate S1 (0.05, 0.1, 0.2, 0.4, 0.6, 0.8 and 1.2 μM, with clamp), with 2 mM dTTP. Due to the mixing of equal volumes, the final concentrations of the reactants were half of the values reported above. The reactants were incubated for varying time (0–80 ms (without clamp), and 0–60 ms (with clamp)) and then quenched with quench buffer. Concentrations of the extended products were then plotted as a function of time and data was fit to a burst equation (Equation 1) shown below:

$$Y = [ED]_A \left((1 - e^{-k_{fast}t}) + (k_{slow}t) \right) + c \qquad (1)$$

where Y is the concentration of extended product, $[ED]_A$ is the amplitude of the fast phase of the time course, and k_{fast} and k_{slow} are the observed rates for the fast and slow phases of the reaction respectively, and c is a constant. Derived amplitudes ($[ED]_A$) of the fast phase from equation (1) were further plotted as a function of DNA substrate concentration for each time course and fit to a quadratic equation (Equation 2) as shown below:

$$[ED]_A = \frac{\left(K_{D,app}^{DNA} + E_A + [DNA]_T\right) - \sqrt{\left(K_{D,app}^{DNA} + E_A + [DNA]_T\right)^2 - 4E_A[DNA]_T}}{2}$$

(2)

where $K_{D,app}^{DNA}$ is the apparent equilibrium dissociation constant for DNA binding, E_A is the active polymerase concentration, and $[DNA]_T$ is the un-extended DNA concentration at the start of the reaction.

A double mixing experiment was performed to determine the apparent dissociation rate (k_{off}) of the PolC•DNA_n complex. The first mixing was set-up such that PolC, 0.1 μM DNA substrate S3 (without clamp) or substrate S1 (with clamp), and β-clamp was mixed with equal volumes

of 96 μM unlabeled DNA substrate (without clamp) or 50 μM unlabeled DNA substrate (with clamp). The reactions were incubated for varying times (0.01–1 s (with clamp), or 0.08–9 s (without clamp)). Following the first mixing, a second mixing with 2 mM dTTP for 28 ms was performed before quenching. Product extension was then plotted as a function of time and data was fit to an exponential function (Equation 3) shown below:

$$Y = Ae^{(-k_{off}t)} + c \qquad (3)$$

where Y is the concentration of extended DNA, k_{off} is the apparent dissociation rate, A is the amplitude, t is the incubation time of the first mixing step, and c is a constant.

To determine the apparent dissociation constant for nucleotide binding to PolC ($K_{D,app}^{dNTP}$), DNA extension reactions were performed as described. For PolC with and without clamp, equal volumes of PolC, 0.1 μM DNA substrate S3 or S1 and β-clamp (in case of with clamp) were mixed with varying nucleotide concentrations (0.78, 1.56, 3.125, 6.25, 12.5, 25 and 50 μM (without clamp), or 0.5, 1, 2.5, 5, 10, 25, 75 and 150 μM (with clamp)) and 50 μM unlabeled DNA. Due to mixing of equal volumes, all reactant concentrations were halved in the final reactions. The reactants were incubated for 0–80 ms before being quenched. Extended products were separated by gel electrophoresis and concentrations of the extended products were plotted as a function of time with time courses being fit to equation (1). The rates of the fast phase (k_{fast}) from equation 1 were plotted as a function of the dNTP concentration and fit to a hyperbolic equation (Equation 4) shown below to determine the maximum rate of nucleotide addition (k_{pol}) and the apparent dissociation constant for binding of nucleotide to PolC ($K_{D,app}^{dNTP}$). Additionally, $K_{D,app}^{dNTP}$ was also determined from the amplitudes (ED_A) of the fast phase of the time courses derived from equation 1, by plotting ED_A as a function of dNTP concentration and fit to a hyperbolic equation (Equation 5) shown below:

$$k_{fast} = \frac{k_{pol}[dNTP]}{K_{D,app}^{dNTP} + [dNTP]} \qquad (4)$$

$$[ED]_A = \frac{[ED]_A^{max}[dNTP]}{K_{D,app}^{dNTP} + [dNTP]} \qquad (5)$$

Multiple nucleotide addition experiments

Multiple nucleotide addition experiments were performed under the same conditions as mentioned for the single nucleotide addition experiments and all extended products were resolved by denaturing TBE polyacrylamide gel electrophoresis. For the correct nucleotides, an equal volume of PolC, β-clamp, and 0.1 μM DNA substrate S1 was mixed with 200 μM dTTP and 200 μM dATP. The reactants were incubated for 0–80 ms before quenching. To constrain the rate constants governing the binding of dATP to the Pol●DNA$_{n+1}$●PP$_i$ complex, primer extension under two additional scenarios were tested. First, PolC, β-clamp, and 0.1 μM DNA substrate S1 was mixed with an equal volume of varying concentrations of dTTP (0.76, 1.5, 3, 6, 12,

24 and 192 μM) and 200 μM dATP. In the second, keeping all other experimental parameters identical to the first, the dTTP concentration was kept constant at 200 μM while dATP concentration was varied (0.76, 1.5, 3, 6, 12, 24 and 192 μM). The reactants were incubated for varying time intervals of 0–80 ms and quenched with quench buffer. In both cases, the final concentration of the reactants (including the dTTP and dATP concentrations) were halved due to mixing. Concentrations of the extended product from all experiments were plotted as a function of time.

To assess the influence of the incorrect nucleotides, DNA extension reactions were performed so that PolC, β-clamp, and 0.1 μM DNA substrate S1 was mixed with an equal volumes of dTTP (5, 10, 20, 50, 150 or 300 μM) and either 400 μM dCTP or dGTP, such that all reactant concentrations were halved in the final reaction mixture. The reactants were incubated for 0–80 ms before quenching. Concentrations of the extended products were plotted as a function of time and globally fit to a single nucleotide addition model.

To measure the rate of processive synthesis by PolC, PolC, β-clamp and 0.1 μM DNA substrate S1 was mixed with an equal volume of 200 μM each of dTTP, dATP, dCTP, dGTP or 200 μM each of dTTP, dATP, dCTP and 96 μM unlabeled DNA trap (without clamp) or 50 μM unlabeled DNA trap (with clamp) and incubated for varying time (0–30 s, without clamp; 0–100 ms, with clamp) before quenching.

Measurement of PP$_i$ release

All stopped-flow assays were performed on a KinTek Corp. (Austin, TX, USA) SF-300X in PolC reaction buffer at 25°C. Pyrophosphate release experiments were performed using a previously described assay (27). All mixtures were incubated for at least 20 minutes before performing the reaction to remove any contaminating phosphate using purine nucleoside phosphorylase (PnPase) and 7-methylguanosine (7-MEG). Equal volumes of 2 μM PolC, 40 μM β monomer, 0.8 μM DNA Substrate S1, 20 μM yeast inorganic pyrophosphatase (PPase), 0.02 U/ml PnPase, and 200 μM 7-MEG were mixed with 200 μM dTTP, 0.02 U/mL PnPase, 200 μM 7-MEG and 2 μM 7-diethylamino-3-((((2-maleimidyl)ethyl)-amino)carbonyl)coumarin)-labeled Phosphate Binding Protein (MDCC-PBP). The sample was excited at 425 nm and fluorescence emission was monitored with a 450 nm long pass filter for 200 ms. We measured the PP$_i$ release rate in the presence of either the next correct or incorrect nucleotide by performing the above-mentioned PP$_i$ release measurement experiment with 200 μM each of dTTP and either dATP (for next correct dNTP), dCTP or dGTP (for next incorrect dNTP).

Data analysis

All DNA extension products resolved by gel electrophoresis were quantified using ImageQuant TL software version 8.1 (GE Healthcare Life Sciences). Data plotting and nonlinear regression were performed using GraphPad Prism version 6.0 (GraphPad Software, San Diego, CA, USA). Global fitting of the data by numerical integration was performed using KinTek Explorer version 10.0.200514 (28).

For the reaction mechanisms accounting for both a single nucleotide and two consecutive nucleotide addition, the forward rate constant of dNTP binding was locked at 100 $\mu M^{-1} s^{-1}$ and the reverse rate constant for PP_i release was locked at 0.001 s^{-1}. PP_i release was modeled as essentially irreversible since the rebinding of PP_i to PolC is negligible under the reaction conditions used. One-dimensional confidence contour analysis was performed using the Fitspace function of KinTek Explorer (29). A X^2 threshold of 0.99 was used, as recommended by the program, to evaluate and determine the 95% confidence intervals for all rate constants for both single and processive synthesis models. From the one-dimensional confidence contour analysis of the processive synthesis addition model, the forward and reverse rate constants of chemistry for the second nucleotide addition step only had lower limits on their values. These rate constants were locked in at their best-fit values for subsequent one-dimensional and two-dimensional confidence contour analysis of the other rate constants in the reaction model.

RESULTS

We determined the kinetic mechanism of *S. aureus* PolC in the presence and absence of its sliding clamp processivity factor, the β subunit of DNA Pol III. The β-clamp is a homodimer that interacts with the C-terminal tail of PolC (Figure 1C) and encircles DNA (16,30). PolC has robust 3′-to-5′ proofreading exonuclease activity (31), so point mutations (D424A, E426A, D509A and D568A) were made in the active site residues of the exonuclease domain (Figure 1C) to prevent degradation of the DNA substrate and to allow us to study the polymerase activity independently. We performed kinetic analysis of PolC under pre-steady state conditions, using comparable concentrations of enzyme and DNA substrate, which allowed us to define each of the key steps involved in a single round of nucleotide addition (Figure 1B). Except where noted otherwise, PolC (with or without β-clamp) and labeled DNA were preincubated together and reactions were then initiated by the addition of a single (or multiple) dNTP (the nucleotide that correctly pairs with the next templating base) and incubated for varying time intervals, usually ranging from 2.5 to 80 ms (Figure 1D). Reactions were terminated by the addition of EDTA to chelate the Mg^{2+} ions required for catalysis and primer-extension products were resolved by denaturing polyacrylamide gel electrophoresis and quantified. DNA substrates consisted of a 5′ fluorescently-labeled primer strand annealed to an unlabeled template strand, forming a DNA duplex of 18 bp with a 5′ single-stranded template region of 19 nucleotides for use in experiments with PolC alone (Substrate S3, Supplementary Figure S1A). This duplex length was chosen based on the crystal structure of PolC bound to DNA (16). For experiments that included the β-clamp, the duplex was extended to 30 or 31 bp (Substrates S1 (Figure 2A) and S2 (Supplementary Figure S2A), respectively), to accommodate both proteins (17). The 5′ single-stranded template region was also extended to 38 nucleotides so that it could potentially interact with the OB domain of PolC (Figure 1C) (16). Pilot experiments showed that the longer DNA did not alter the nucleotide incorporation kinetics of PolC alone (data not shown).

β-clamp stabilizes PolC binding to DNA

PolC displays biphasic reaction kinetics (Figure 2B and Supplementary Figure S1B), consistent with the chemical step of bond formation (Figure 1B, step 3) being followed by a slower post-chemistry step. In the initial exponential fast phase, the pre-bound fraction of the DNA substrate quickly converts to product. The slow post-chemistry step limits the rate of subsequent rounds of nucleotide addition, resulting in the second, slower phase.

Since the fast phase of product formation represents the incorporation of dNTP by the preformed binary complex (Pol•DNA_n) (Figure 1B, steps 2–3), the amplitudes of this phase, obtained by fitting the data to the burst equation (Equation 1), represent the amount of Pol•DNA_n complex that can productively be converted into product upon dNTP addition. We determined the apparent dissociation constant for the formation of the Pol•DNA_n complex ($K_{D,app}^{DNA}$) by re-plotting the fast phase amplitudes as a function of DNA concentration (Figure 2C and Supplementary Figure S1C) and fitting the data by non-linear regression to a quadratic equation (Equation 2). We found that the β-clamp processivity factor increases the affinity of PolC for DNA by ~4-fold, even on these linear substrates where the clamp is not topologically constrained. The $K_{D,app}^{DNA}$ for PolC is 126 ± 8 nM in the presence of clamp (Figure 2C) and 472 ± 282 nM in its absence (Supplementary Figure S1C).

For all the replicative DNA polymerases studied to date using steady-state kinetic methods, the slow step in a single nucleotide incorporation cycle corresponds to dissociation of the post-chemistry binary complex (Pol•DNA_{n+1}; Figure 1B, step 5), releasing the DNA polymerase so that it can bind a new DNA substrate and perform a second round of nucleotide incorporation. When compared to previously characterized DNA polymerases, PolC binds to the DNA substrate relatively weakly, which could result from either slow binding of the polymerase to the DNA (governed by k_1, the forward rate constant for step 1, Figure 1B) or rapid dissociation of the PolC•DNA_n complex (governed by k_{-1}, the reverse rate constant for step 1, Figure 1B).

We measured the dissociation rate (k_{off}) of the PolC•DNA_n complex by performing a double-mixing experiment in the presence (Figure 2D) or absence (Supplementary Figure S1D) of β-clamp. PolC and fluorescently labeled DNA substrate were pre-incubated together and then mixed with excess unlabeled DNA (DNA substrate S1) and incubated for varying time intervals. After the first incubation, a saturating amount of dTTP was added and the reaction was terminated after 28 ms. Any enzyme that dissociates from the labeled DNA will bind to the unlabeled trap DNA and will not contribute to detectable product formation. The labeled DNA that remained bound to PolC after the first incubation is then extended by a single nucleotide during the second incubation. Concentrations of the labeled DNA product extended by a single nucleotide were plotted as a function of the first incubation time (Figure 2D and Supplementary Figure S1D). The product decreased exponentially with time, indicating that PolC dissociated from the labeled DNA substrate with increasing time and became trapped by the unlabeled DNA. The data were fit to a single exponential equation (Equation 3) and
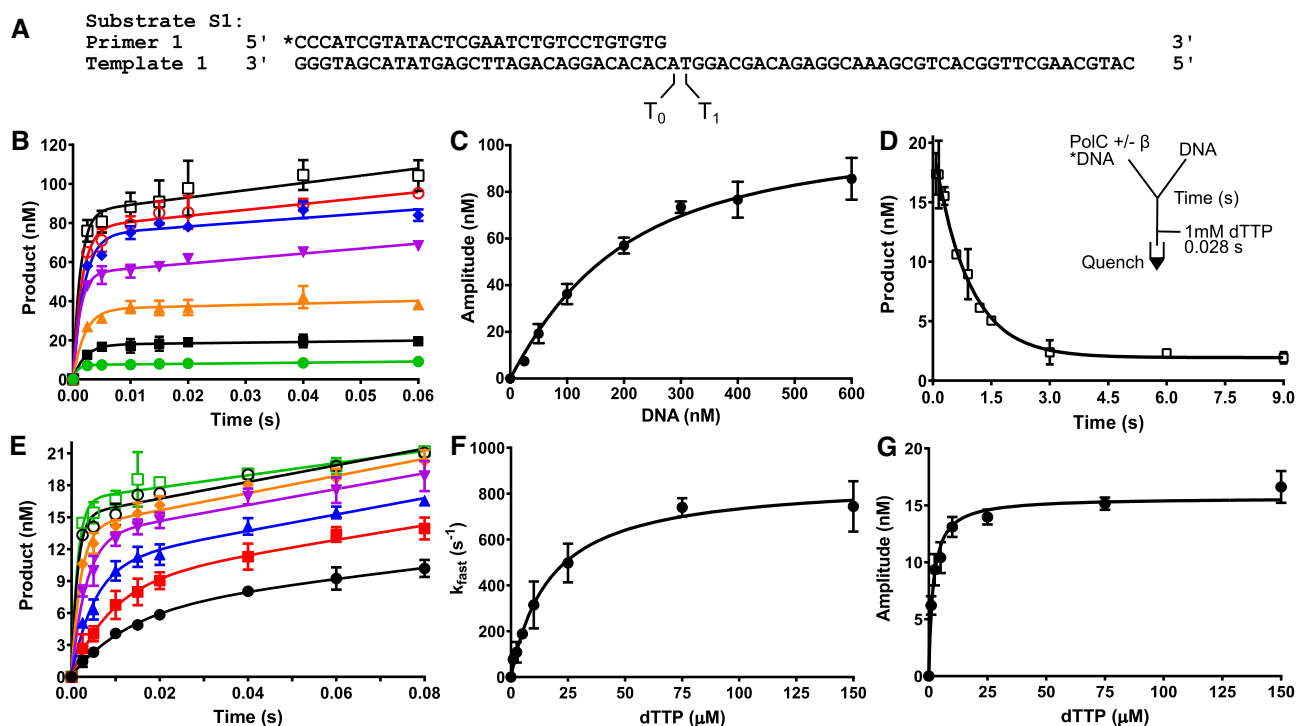
Figure 2. PolC has weak affinity for DNA and chemistry of nucleotide addition is reversible. (**A**) DNA substrate S1 used in DNA extension experiments composed of primer 1 and template 1. Primer 1 has a 5′ FAM label (*). (T_0): the first templating base; (T_1): the second templating base. (**B**) Time courses from DNA extension assays performed with various substrate S1 concentrations. Final concentrations of 500 nM PolC, 10 μM β-clamp, and various concentrations of DNA substrate S1 (● 25, green; ■ 50, black; ▲ 100, orange; ▼ 200, magenta; ♦ 300, blue; ○ 400, red and □ 600 nM, black) were mixed with a final concentration of 1 mM dTTP. The reactants were incubated for various timepoints (0–60 ms) and quenched with EDTA and formamide. Extended product concentration was plotted as a function of time and fitted to Equation (1). (**C**) Plot of the amplitudes of the fast exponential phase of the time courses from (B) as a function of substrate concentration with data fitted to Equation (2). $K_{D,app}^{DNA}$ was found to be 126 ± 18 nM and active PolC to be 108 ± 5 nM (R^2: 0.98). (**D**) Time course from the double mixing experiment performed to determine the rate of DNA dissociation from the PolC•DNA$_n$ complex. Inset shows the assay setup. The assay was initiated by mixing final concentrations of 110 nM active PolC, 10 μM β-clamp, and 50 nM DNA substrate S1 with 25 μM unlabeled trap DNA and incubating for varying time (0.08–9 s). A second mixing followed this where 1 mM dTTP (final concentration) was incubated with the other reactants for 28 ms prior to quenching. The amount of extended product was plotted as a function of the first incubation time and fitted to Equation (3). The rate of decline of product formed was found to be 1.1 ± 0.1 s^{-1} (R^2: 0.97) and is equivalent to the dissociation rate (k$_{off}$) of PolC from substrate S1. (**E**) DNA extension time courses with various dTTP concentration. Final concentrations of 110 nM active PolC, 10 μM β-clamp, and 50 nM labeled DNA substrate S1 were mixed with various concentrations of dTTP (● 1, black; ■ 2.5, red; ▲ 5, blue; ▼ 10, magenta; ♦ 25, orange; ○ 75, black and □ 150 μM, green) and 25 μM unlabeled trap DNA. Reactants were incubated for varying time (0–80 ms) before quenching. Concentration of extended product was plotted as a function of time and fitted to Equation (1) to determine the rate and amplitude of the fast phase. (**F**) Plot of the observed rates (k$_{fast}$) of the fast phase versus dTTP concentration. Data were fit to Equation (4) to give $K_{D,app}^{dNTP}$: 17.0 ± 2.6 μM, and the maximum rate of chemistry, k$_{pol}$: 859 ± 39 s^{-1} (R^2: 0.96). (**G**) Plot of the amplitudes of the fast phase versus dTTP concentration. Data was fit to Equation (5) and the $K_{D,app}^{dNTP}$ was found to be 1.9 ± 0.2 μM. R^2: 0.96. Means and standard deviations (SDs, error bars) were calculated from at least three replicates. ±: standard error of the mean (SEM).

the rates for dissociation of PolC from DNA (k$_{off}$) were calculated to be 1.1 ± 0.1 s^{-1} (Figure 2D) and 7.4 ± 3.0 s^{-1} (Supplementary Figure S1D) in the presence and absence, respectively, of β-clamp.

Although the processivity factor stabilizes DNA binding by ∼7-fold, dissociation of DNA from PolC is one- to two-orders of magnitude faster than for other DNA polymerases with their processivity factors. For example, DNA dissociates from phage T7 DNA polymerase and mammalian polymerase delta with rates of 0.2 s^{-1} (10) and 0.006 s^{-1} (32), respectively. Since the equilibrium dissociation constant (K_D^{DNA}) for a one step binding reaction can be expressed as a ratio between the association and dissociation rate constants (k$_1$ and k$_{-1}$, respectively), the apparent association rate constant (k$_{1,app}$) can be estimated to be 15.7 μM^{-1} s^{-1} for PolC alone and 8.7 μM^{-1} s^{-1} for PolC in the presence of β-clamp, if we approximate the dissociation rate k$_{off}$ to

be the dissociation rate constant, k$_{-1}$. Thus, association of PolC with DNA is in the 10^5–10^6 M^{-1} s^{-1} range, as expected for diffusion-limited macromolecular interactions (33), and the rapid dissociation of the binary complex is responsible for the weak binding affinity between PolC and DNA.

Phosphodiester bond formation is fast but reversible

The affinity of the incoming dNTP for the Pol•DNA$_n$ complex can be determined from the increase in the rate of DNA extension with increasing concentrations of nucleotide. Typically, these experiments are performed under conditions where all of the substrate DNA is bound by the polymerase, limiting the reaction to a single turnover (34,35). However, due to the weak $K_{D,app}^{DNA}$ and low active fraction of PolC, we were unable to saturate DNA binding. Instead, single turnover conditions were achieved by includ-

ing excess unlabeled DNA in the dNTP solution to act as a trap and prevent PolC from re-binding to the labeled DNA after catalyzing a single round of nucleotide addition.

Surprisingly, even though polymerase turnover was prevented by the addition of unlabeled DNA trap, the time courses of single-nucleotide addition were biphasic, both in the presence and absence of β-clamp (Figure 2E and Supplementary Figure S1E). The data were fit to a burst equation (Equation 1) to determine the rate of the nucleotide incorporation and the amplitude of the fast phase. The observed rates (k_{fast}) of the fast phase were plotted as a function of dTTP concentration (Figure 2F and Supplementary Figure S1F) and the data were fit to a hyperbolic equation (Equation 3) to determine the apparent equilibrium dissociation constant of the incoming nucleotide from the Pol•DNA$_n$•dNTP complex ($K_{D,app}^{dNTP}$) and the maximum rate of polymerization (k_{pol}). We also found that the amplitude of the fast phase increased hyperbolically with increasing dTTP concentration (Figure 2G and Supplementary Figure S1G). These reaction kinetics are not specific to dTTP, as we observed the same behavior when dATP is the incoming nucleotide (Supplementary Figure S2). Overall, nucleotides bind tightly ($K_{D,app}^{dNTP}$ of 2–20 μM) to PolC and are incorporated rapidly (k_{pol} of 350–860 s^{-1}), both in the absence (Supplementary Figure S1E–G) and presence (Figure 2 and Supplementary Figure S2) of β-clamp.

The biphasic reaction kinetics and the hyperbolic dependence of the fast phase amplitude on nucleotide concentration indicate that the chemical step of bond formation is reversible and is in equilibrium with nucleotide binding, assuming dNTP binding to the Pol•DNA$_n$ complex equilibrates rapidly (Figure 1B, steps 2–3), as would be expected for diffusion-limited binding of a small molecule ligand to a macromolecule (36). Moreover, for such an equilibrium to be established, bond formation must be followed by a slower step, which can be attributed to the post-chemistry steps leading to the release of pyrophosphate (PP$_i$) byproduct (Figure 1B, step 4). Slow PP$_i$ release would account for the slower phase of the reaction that occurs even in the presence of the unlabeled DNA trap (Figure 2E). This behavior of PolC is markedly different from the DNA polymerases studied to date, where the polymerase commits to the DNA extension step by rapidly releasing PP$_i$ after bond formation (10), although fast PPi has been observed with DNA polymerization catalyzed by HIV reverse-transcriptase with an RNA template (37,38).

Slow pyrophosphate release limits the rate of single nucleotide addition

To test our hypothesis that PP$_i$ release is the slow step after chemistry, we directly measured the PP$_i$ release rate experimentally, using a fluorescence-based coupled-reaction assay that has been described previously (27). Briefly, yeast inorganic pyrophosphatase hydrolyzes the PP$_i$ byproduct of the DNA polymerase reaction, releasing two molecules of P$_i$ that then bind to a fluorescently labeled *E. coli* phosphate binding protein. In the absence of pyrophospatase, no fluorescence signal is observed (Supplementary Figure S5A), demonstrating this assay measures PP$_i$ release and not the production of P$_i$ by some other mechanism. The

fluorescence trace from the coupled-reaction assay (Figure 3A), together with the time-courses from the DNA extension experiments (Figure 3B–D), were analyzed using KinTek Explorer software (28). This allowed global fitting of all experiments simultaneously through numerical integration based on a single kinetic model, without making any of the simplifying assumptions that are typically required to fit the data analytically using equations. The rate constants derived from global fitting are constrained by the data, as indicated by confidence contour analysis showing defined upper and lower boundaries (Supplementary Figures S3 and S4, Supplementary Tables S1 and S2).

In the kinetic scheme for addition of a single nucleotide by PolC with β-clamp (Figure 3E), dNTP binding to the Pol•DNA$_n$ complex was followed by a reversible step of phosphodiester bond formation followed by PP$_i$ release. PP$_i$ release was modeled as unidirectional, since the amount of PP$_i$ generated during these reactions would be too low to drive the rebinding of pyrophosphate to the Pol•DNA$_{n+1}$ complex. We note here that it is possible for additional reaction intermediates to exist, especially after dNTP binding (Figure 3E, step 2) and before PPi release (Figure 3E, step 4). PolC almost certainly undergoes a conformational change upon binding dNTP and releasing PP$_i$ (16), but in the absence of experimental data addressing these possibilities, we only considered the minimal kinetic scheme that is shown in Figure 3E. Moreover, the rate of a possible conformational change is expected to be faster than chemistry (6,7), and thus will not contribute to the overall kinetics of the catalytic cycle.

The kinetic constants governing this pathway were determined by globally fitting the PP$_i$ release fluorescence trace (Figure 3A) and the DNA extension time-courses (Figure 3B–D). K_D^{DNA} and K_D^{dNTP} were determined to be 313 nM and 7 μM, respectively (Figure 3E and Supplementary Table S1). According to this analysis, bond formation (Figure 3E, step 3) is reversible, as predicted from the quench-flow experiments, with a forward rate constant (k_3) of ~550 s^{-1} and a reverse rate constant (k_{-3}) of ~260 s^{-1} (Figure 3E). Thus, the maximum rate of the chemical step (k_{pol}) obtained is ~810 s^{-1} ($k_{pol} = k_3 + k_{-3}$).

Global fitting of the data directly demonstrates that phosphodiester bond formation is indeed fast and is followed by slow pyrophosphate release. The rate constant determined for PP$_i$ release (k_4) is ~19 s^{-1}, more than an order of magnitude slower than the reverse rate of phosphodiester bond formation (k_{-3}). This is the crucial feature responsible for the establishment of an equilibrium between the steps of nucleotide binding and the chemistry step, which depends on the slow PP$_i$ release (Figure 3E, steps 2–3).

The next correct nucleotide accelerates pyrophosphate release

The kinetic mechanism that we have determined for the incorporation of a single nucleotide by PolC (Figure 3E) presents a conundrum: how can *S. aureus* DNA replication proceed at rates of up to 1000 nucleotides per second (39–41) when PP$_i$ release needs to occur for each nucleotide added and would limit the rate of processive DNA synthesis to ~20 nucleotides per second? To determine the
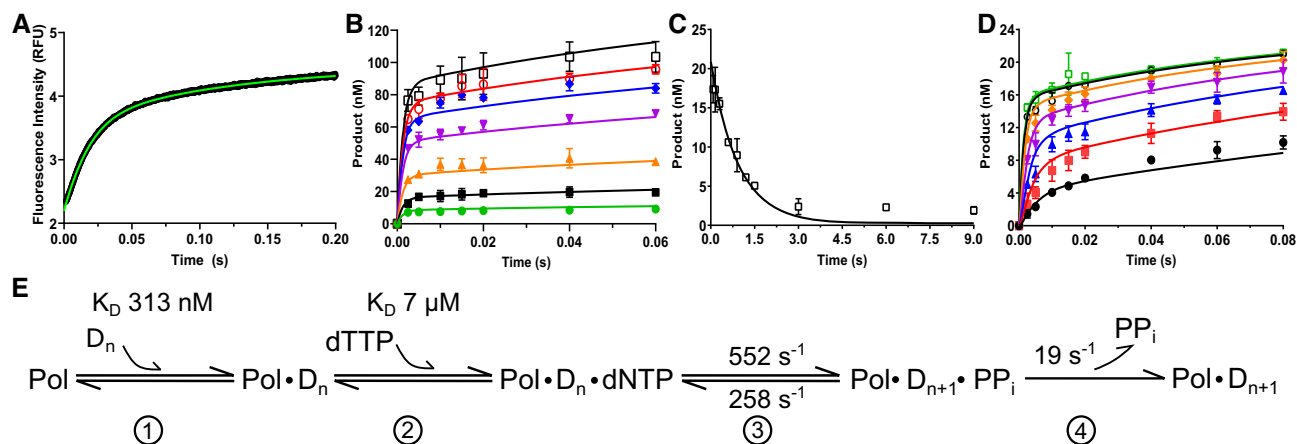
Figure 3. Global fitting of single nucleotide addition reveals PP_i release is slow. (**A**) Fluorescence time course from the coupled assay to measure the PP_i release rate during addition of dTTP. (**B**) DNA extension time courses from Figure 2B. (**C**) Double mixing experiment to measure the dissociation of PolC from Figure 2D. (**D**) DNA extension time courses from Figure 2E. In panels A–D, the smooth lines overlaying the symbols represent the best global fit of the data to the unifying kinetic scheme. (**E**) Kinetic scheme used to globally fit the data displayed in panels A–D with KinTek Explorer. Best fit values for each first-order rate constant and equilibrium constant are indicated. The forward rate constant of nucleotide binding (k_2) was locked in at a diffusion limited rate of $100\ \mu M^{-1}\ s^{-1}$ and then fitting to derive estimates for k_{-2} were used to compute K_D^{dTTP}.

speed of processive DNA synthesis by PolC, we performed a primer extension assay using all four nucleotides. Excess unlabeled DNA was added along with the nucleotides to ensure that extended products were generated only from processive DNA synthesis. Under these conditions, PolC with β-clamp was able to reach the end of the substrate by adding at least 38 nucleotides within 40 ms (Supplementary Figure S1H, left). The β-clamp did not play a role in accelerating processive synthesis by PolC because even in the absence of the clamp, PolC could add at least 14 nucleotides in 10 ms (Supplementary Figure S1H, right). This suggests that during processive synthesis the rate of PP_i release must increase dramatically. To better quantify the processive rate, we repeated the previously described experiment with only three of the nucleotides, which would result in DNA substrate S1 getting extended by five nucleotides (Figure 2A). PolC was able to add five nucleotides within 2.5 milliseconds as observed by denaturing polyacrylamide gel electrophoresis (Figure 4A). The products formed were quantified and fit using KinTek Explorer (Figure 4B). The rates corresponding to addition of each respective nucleotide were averaged together to give a processive synthesis rate of ~600 nucleotides per second, a DNA extension rate consistent with the reported rate of bacterial replication, but faster by more than an order of magnitude than the predicted processive synthesis rate from the single nucleotide addition experiments.

Taken together, this suggests that a mechanism to stimulate PP_i release from PolC must exist when other nucleotides are present. To elucidate how this could occur, we analyzed the simplest case of processive synthesis: addition of two consecutive nucleotides. The first and second nucleotides to be added to the growing primer strand of DNA substrate S1 (Figure 2A) are dTTP and dATP that respectively pair with the first (T_0) and the second (T_1) templating bases. When just these two nucleotides were included in a primer extension reaction, we observed two additional bands above the band corresponding to the un-extended primer, even at

the first 2.5 ms timepoint (Figure 4C). Since the second nucleotide (dATP) cannot be added to the DNA substrate until the PP_i generated during the first nucleotide (dTTP) addition cycle is released and PolC has translocated by one nucleotide along the DNA template strand, a processive synthesis rate of ~600 s^{-1} (Figure 4D) can only be supported by a PP_i release rate that is much faster than ~20 s^{-1}. Moreover, we have verified that PolC cannot erroneously add dATP instead of dTTP as the first nucleotide (Supplementary Figure S5B). Clearly, the kinetic parameters derived from the addition of a single nucleotide (Figure 3E) do not account for how rapidly the two nucleotides are incorporated (Figure 4D, compare dashed lines with plotted data points).

To determine whether any second nucleotide or just the next correct nucleotide could accelerate PP_i release, we followed the kinetics of dTTP incorporation in DNA substrate S1 and the corresponding PP_i release, as in figures 2E and 3A respectively, but in the presence of a saturating amount (200 μM) of either dCTP (Figure 5A and C) or dGTP (Figure 5B and D), which do not base pair with the templating bases T_0 and T_1. We observed that the primer strand was extended by a single nucleotide indicating that PolC did not mis-incorporate dCTP or dGTP after dTTP addition. In separate control experiments (Supplementary Figure S5B), we verified that PolC does not mis-incorporate dCTP or dGTP opposite T_0 under our experimental conditions. The concentrations of the extended DNA from the primer extension assays and the fluorescence traces from the coupled reaction assays were plotted as a function of time and the data was fitted globally to a single nucleotide incorporation model (Figure 5E and F; Supplementary Figures S6 and S7; Supplementary Tables S3 and S4). We observed that in the presence of the incorrect nucleotide (dCTP or dGTP) the chemistry step remains fast and reversible (k_{pol}: 734 s^{-1} in the presence of dCTP and 834 s^{-1} in the presence of dGTP) followed by a slow PP_i release (23 s^{-1} in the presence of dCTP and 30 s^{-1} in the presence of dGTP), indicating that the incorrect nucleotides do not influence the dTTP incor-
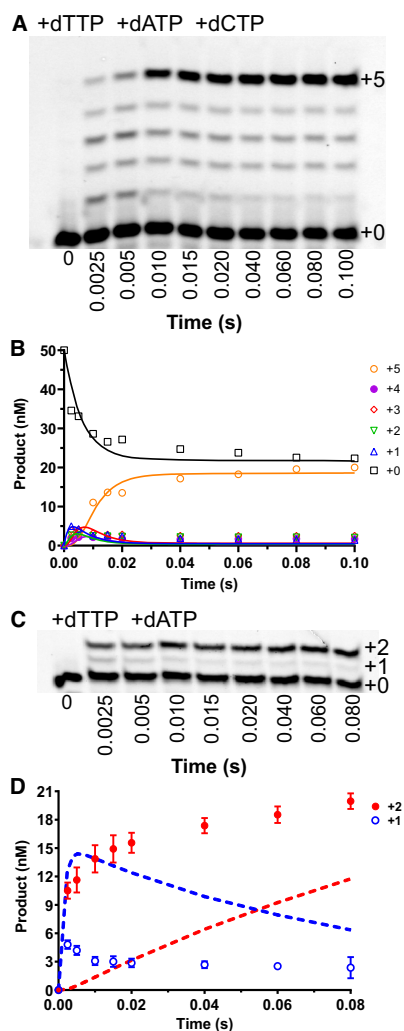
Figure 4. Processive synthesis by PolC is fast. (**A**) Representative denaturing polyacrylamide gel depicting multiple nucleotide incorporation during processive synthesis by PolC in the presence of the β-clamp processivity factor. The DNA extension assay was performed with final concentrations of 110 nM active PolC, 10 μM β and 50 nM DNA substrate S1, 100 μM each of dTTP, dATP, dCTP, and 25 μM unlabeled DNA substrate. The reactants were incubated for varying timepoints (0–100 ms). Fully extended products are observed by 2.5 milliseconds. +0: un-extended primer strand, +5: primer strand extended by five nucleotides. (**B**) Representative time course of the DNA extension shown in panel A. Primer extension by up to five nucleotides (△ +1, blue; ▽ +2, green; ◇ +3, red; ● +4, purple; ○ +5, orange) was globally fit using KinTek Explorer with smooth lines representing the best fit to the data. The rates of nucleotide addition were averaged for a processive synthesis rate of 604 nucleotides per second. (**C**) Denaturing TBE acylamide gel depicting two consecutive dNTP incorporation reactions by PolC in the presence of the β-clamp processivity factor. This represents the simplest experiment to assess processive synthesis. The DNA extension assay was performed with final concentrations of 110 nM active PolC, 10 μM β-clamp and 50 nM DNA substrate S1 mixed with a final concentration of 100 μM each of dTTP and dATP and the reactants were incubated for varying timepoints (0–80 ms). (**D**) Time course of the DNA extension shown in panel C. Primer extension by one (○ +1, blue) or two (● +2, red) nucleotides representing dTTP (+1) and dATP (+2) incorporation, respectively, plotted separately. Dashed lines represent the results expected from simulation of product formation during addition of two nucleotides based on the rate constants governing a single nucleotide incorporation by PolC (shown in Figure 3E) with reversible chemistry and slow release of PP$_i$ (k$_3$: 552 s^{-1}, k$_{-3}$: 258 s^{-1}, k$_4$: 19 s^{-1}). The blue dashed line represents +1 product, while the red dashed line shows predicted +2 product. Reactions were performed in triplicate.

poration kinetics. Taken together, our results show that only the presence of the next correct nucleotide stimulates PP$_i$ release during processive synthesis by PolC.

PolC can sense the identity of the next incoming nucleotide

Since only the next correct incoming nucleotide (and not the incorrect ones) facilitate PP$_i$ release, we hypothesized that the next correct nucleotide (dATP) must bind to the post-chemistry ternary complex formed after addition of the first nucleotide (dTTP). Based on this hypothesis, we developed the kinetic scheme for processive DNA synthesis by PolC that is shown in Figure 6A and tested the model by global data fitting using KinTek Explorer. The crucial difference between this pathway and previously proposed kinetic mechanisms of processive synthesis (42) lies in the fact that, for PolC, release of the PP$_i$ generated after dTTP incorporation can occur by two pathways instead of just one. In the standard pathway, PP$_i$ release occurs before dATP binding (Figure 6A, steps 4 and 5) while in the alternative pathway, PP$_i$ release occurs after dATP binding (Figure 6A, steps 6 and 7).

Global fitting of the nucleotide addition and PP$_i$ release time-courses demonstrates that the proposed processive synthesis model is sufficient to explain our experimental results (Figure 6). In addition to the primer-extension (Figure 6B) and PP$_i$ release (Figure 6C) experiments that included equal concentrations of dTTP and dATP (100 μM each), we performed two more primer extension experiments to constrain the rate constants of the different steps of the new scheme. The first experiment was designed to measure the affinity of dTTP for the Pol•DNA$_n$ complex by varying the concentration of dTTP (as in Figure 2E), but in the presence of 100 μM dATP (Figure 6D and E). In the second experiment the concentration of dATP was varied from 0.38 to 96 μM, while the concentration of dTTP was kept at 100 μM (Figure 6F and G). For each experiment, the product corresponding to the addition of each nucleotide was plotted independently as a function of time (dTTP addition, Figure 6D and F; dATP addition, Figure 6E and G).

The rate constants derived from globally fitting these data demonstrate that dATP (the next correct nucleotide) dramatically accelerate the dissociation of the PP$_i$ byproduct generated from the incorporation of dTTP, such that the alternate pathway that proceeds through a Pol•DNA$_{n+1}$•PP$_i$•dATP quaternary complex becomes the preferred pathway for processive DNA synthesis (Figure 6A, green; Supplementary Figure S8 and S9; Supplementary Table S5). In this scenario, the rate constant (k$_7$) for PP$_i$ release is at least 1230 s^{-1} (Figure 6A, step 7) and is no longer rate-limiting. Rapid PP$_i$ release precludes the formation of an equilibrium between binding of the first nucleotide (Figure 6A, step 2) and its incorporation into the DNA substrate (Figure 6A, step 3). Addition of the second nucleotide is fast and reversible (Figure 6A, step 8) but, crucially, release of the second PP$_i$ is slow (Figure 6A, step 9). This is consistent with our model since the presence of the next *correct* nucleotide is needed to accelerate PP$_i$ release. The rate of dATP addition (Figure 6A, step 8) is not well constrained by the data, and only lower limits on the for-
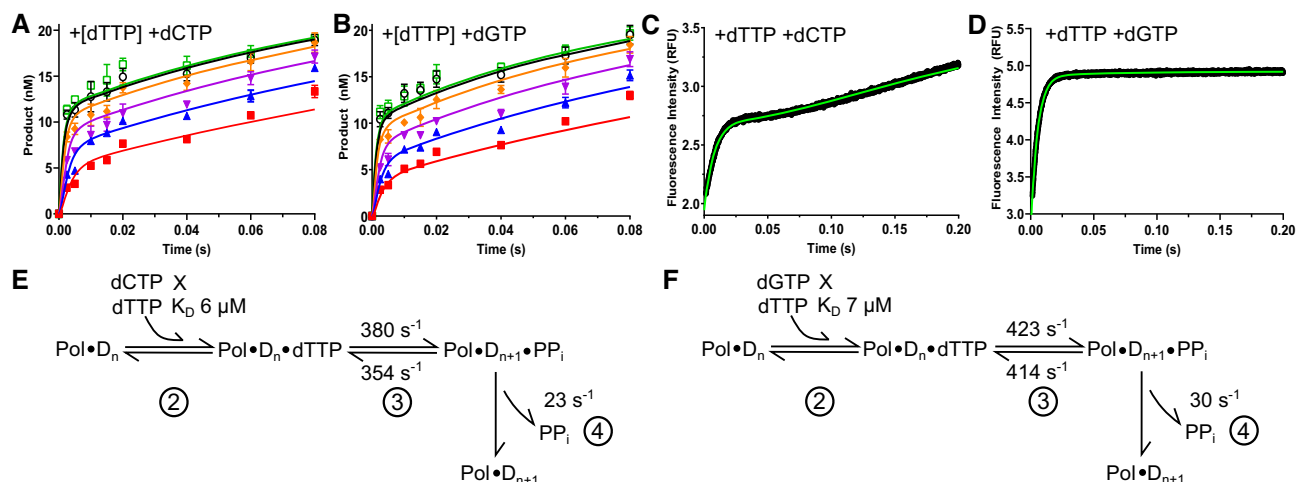
Figure 5. Presence of incorrect nucleotides does not speed up release of PP_i. (**A**, **B**) Time courses from DNA extension assays performed with final concentration of 110 nM active PolC, 10 μM β-clamp and 50 nM labeled DNA substrate S1 mixed with various dTTP concentrations (■ 2.5, red; ▲ 5, blue; ▼ 10, magenta; ♦ 25, orange; ○ 75, black and □ 150 μM, green), 200 μM dCTP or dGTP and 25 μM unlabeled trap DNA. Reactants were incubated for varying time (0–80 ms) before quenching. Extended product was plotted as a function of time and fitted to Equation (1) to determine the rate and amplitude of the fast phase. (**C**, **D**) Fluorescence trace from the coupled assay to measure PP_i release by PolC in a reaction containing both 100 μM dTTP and dCTP or dGTP. (**E**, **F**) Kinetic scheme used to globally fit the data displayed in panels A–D with KinTek Explorer. Best fit values for each first-order rate constant and equilibrium constant are indicated. The forward rate constant of nucleotide binding (k_2) was locked in at a diffusion limited rate of 100 $\mu M^{-1} s^{-1}$ and then fitting to derive estimates for k_{-2} were used to compute K_D^{dTTP}. X: indicates the presence of the incorrect nucleotide that does not get incorporated, and the equilibrium binding constant is unknown. Reactions were performed in triplicate.

ward and reverse rate constants could be established (k_8 and k_{-8}, Figure 6A, Supplementary Table S5), resulting in a k_{pol} of at least 1500 s^{-1}, which is more than adequate to explain the observed rates of DNA synthesis *in vitro* and *in vivo*.

In summary, our results indicate that after the addition of the first nucleotide opposite the T_0 base of the template strand (Figure 2A), the post-chemistry ternary complex (Pol•DNA$_{n+1}$•PP_i, Figure 2A, step 3) can interact with and recognize the next correct incoming nucleotide (which will be incorporated opposite to the T_1 base of the temple strand). This recognition triggers rapid release of the PP_i byproduct generated from the first round of nucleotide addition. Using this mechanism, PolC can successfully perform the rapid processive DNA synthesis essential for bacterial replication.

DISCUSSION

The kinetic mechanism of a bacterial replicative DNA polymerase

Our transient-state kinetic characterization of *S. aureus* PolC has revealed a surprising mechanism by which the polymerase can sense the presence of the next correct dNTP prior to fully committing to incorporation of the current dNTP. In a single dNTP incorporation cycle, PP_i release is ∼40-fold slower than the maximal rate of nucleotide addition (∼20 s^{-1} versus ∼800 s^{-1}). However, we find that this bottleneck to rapid DNA replication is relieved when PolC is provided with the next correct dNTP, binding of which accelerates dissociation of the PP_i that was generated during the current nucleotide cycle to the point where PP_i release no longer limits the rate of polymerization. Thus, PolC can perform processive DNA synthesis at speeds compara-

ble to that of a fully assembled replication complex (41). Slow PP_i release in the absence of the next correct dNTP is an intrinsic property of PolC, as it does not depend on association with the β-clamp, nor does it depend on either the N-terminal or exonuclease domains of the polymerase (25). Steady-state analysis of two Y-family DNA polymerases suggest that PP_i is hydrolyzed at the polymerase active site prior to release (43,44). However, this is clearly not a general phenomenon as PolC does not hydrolyze PP_i to Pi on a timescale that is relevant to nucleotide incorporation (Supplementary Figure S5A).

The evolutionarily unrelated polymerases human Pol γ, HIV-1 reverse transcriptase (HIV-RT), Hepatitis C Virus (HCV) RNA-dependent RNA polymerase NS5B, and T7 DNA polymerase have displayed similar kinetics in specific contexts. Human Pol γ demonstrates reversible chemistry and slow PP_i release when incorporating various azido-modified nucleotide analogs and 8-oxo-7,8-dihydroguanosine 5′-triphosphate (8-oxo-dGTP) (45,46). HIV-RT demonstrates slow PP_i release during both nucleotide misincorporation and processive synthesis in the presence of all four cognate nucleotides when utilizing an RNA template (37). HCV NS5B has demonstrated reversible chemistry and slow PP_i release during nucleotide misincorporation (47). Recently, T7 DNA polymerase was shown to be partially limited by slow PP_i release at low temperature (7). However, in no case has the next correct nucleotide been implicated as the regulator of the polymerase catalytic cycle.

To our knowledge this is the first report of a kinetic mechanism that allows a DNA-dependent DNA polymerase to sense the presence of the next correct nucleotide prior to completion of the catalytic cycle of the current nucleotide addition. It remains to be seen whether this mechanism is
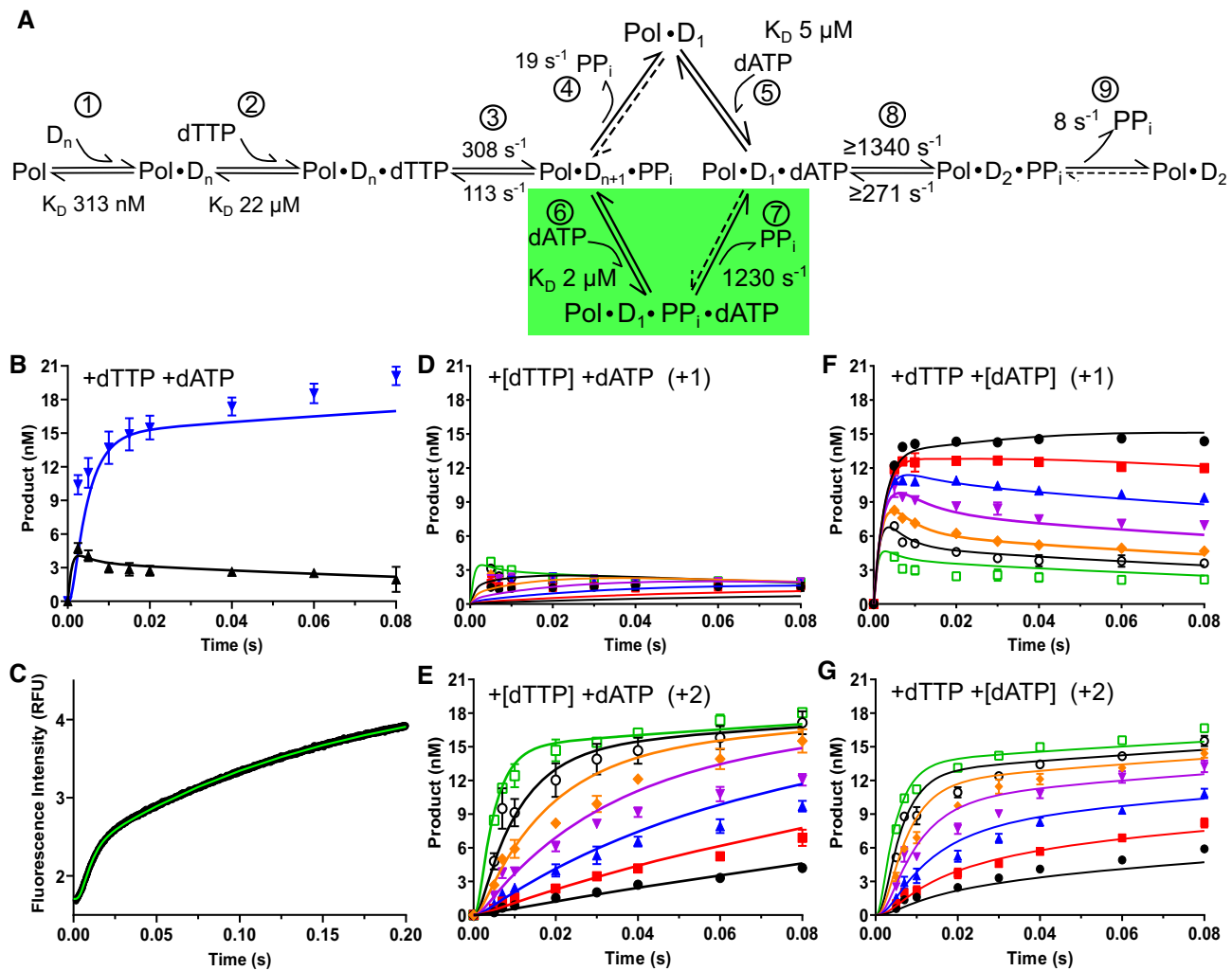
Figure 6. Global data fitting reveals that the next correct nucleotide speeds up release of PP_i. (**A**) Kinetic scheme of processive synthesis by PolC used to globally fit time courses in panels B–G. The scheme includes two kinetic routes for addition of dNTP when the second correct nucleotide is present. Best fit values of the rate and equilibrium constants are indicated for each reaction step. Only lower limits could be established for the forward and reverse rate constants of the chemistry step for the second nucleotide addition (step 8). The rate constant governing the release of PP_i byproduct after addition of the first nucleotide (step 4) was fixed at 19 s^{-1} (Figure 3). (**B**) Globally fit DNA extension time courses from Figure 4D, where PolC was mixed with both 100 μM dTTP and dATP. (**C**) Fluorescence trace from the coupled assay to measure PP_i release by PolC in a reaction containing both 100 μM dTTP and dATP. (**D, E**) DNA extension assay where final concentrations of 110 nM active PolC, 10 μM β-clamp and 50 nM DNA substrate S1 were mixed with various concentrations of dTTP (● 0.38, black; ■ 0.75, red; ▲ 1.5, blue; ▼ 3, magenta; ♦ 6, orange; ○ 12, black and □ 96 μM, green) and 100 μM dATP with the bands for dTTP (+1) and dATP (+2) addition plotted separately in (D) and (E), respectively. (**F, G**) DNA extension time courses where final concentrations of 110 nM active PolC, 10 μM β-clamp, and 50 nM DNA substrate S1 were mixed with 100 μM dTTP and various dATP concentrations (● 0.38, black; ■ 0.75, red; ▲ 1.5, blue; ▼ 3, magenta; ♦ 6, orange; ○ 12, black; and □ 96 μM, green) with the extended bands for addition plotted separately in (F) and (G), respectively. Smooth lines in panels B–G represents the best fit generated during global data fitting. Reactions were performed in triplicate.

unique to PolC or extends to the C-family of DNA polymerases and to DNA polymerases from other families, but there are some hints that it may (32,48). Remarkably, a similar kinetic mechanism of regulation has been proposed for the DNA-dependent RNA polymerase from *E. coli*. When incorporating a single nucleotide during transcription, release of pyrophosphate is slow, thus governing the overall rate of elongation (49). However, there is evidence for an allosteric templated binding site for the next correct nucleotide, which leads to a post-chemistry conformational change that speeds up the release of pyrophosphate (50–52). Our kinetic data demonstrates that PolC must also have a mechanism to allow the next correct nucleotide to interact

with the next templating base to speed up the release of pyrophosphate.

Structural insights into the mechanism of PP_i release

The crystal structure (Figure 7A) of PolC from the thermophilic bacterium *G. kaustophilus* (Gka-PolC) (16) provides some key insights into how formation of a new base pair can be coupled to the previous catalytic cycle. Since PP_i release is stimulated by the next correct (but not incorrect) dNTP, we predict that there is a pre-insertion binding site for the next correct dNTP where the base can form a Watson-Crick pair with the next templating base (T_1), prior
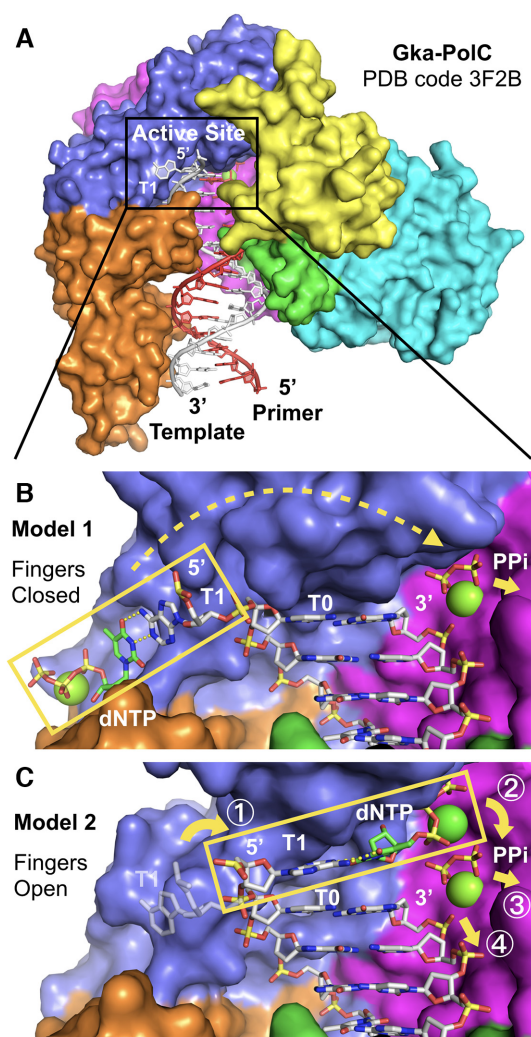
Figure 7. Structural models for the stimulation of PPi release by binding of the next correct nucleotide. (**A**) Overview of the *G. kaustophilus* PolC ternary complex crystal structure (PDB code 3F2B) highlighting the active site. (**B**) Structural model of the next correct dNTP (green) pairing with the next templating base (T1) after addition of a nucleotide (paired with the current templating base (T0)) to the 3′ end of the primer strand with the fingers in the closed conformation. An allosteric interaction (dotted yellow line) between the pre-insertion binding site (yellow rectangle) and the catalytic site would trigger PP_i release. (**C**) Structural model of the next correct dNTP (green) pairing with the templating base (T1) after opening of the fingers domain but prior to the release of the $PP_i \bullet Mg^{2+}$. The next templating base (T1) would rotate into the pre-insertion binding site (yellow rectangle) from the flipped-out configuration (translucent grey) to pair with the next correct dNTP (step 1). Competition of the dNTP and associated Mg^{2+} (green sphere) for binding to the catalytic aspartates (step 2), would trigger PP_i release (step 3), and would likely be associated with closing of the fingers domain and translocation of the DNA duplex (step 4).

to release of the PP_i formed in the current nucleotide incorporation cycle. The Gka-PolC structure shows the polymerase poised for nucleotide incorporation, with the incoming dNTP forming a correct Watson-Crick pair with the templating base T_0 and the 3′ end of the elongating DNA strand positioned at the active site for catalysis. The next base to be replicated is swung out of the active site and,

as shown in model 1 (Figure 7B), it is positioned where it could potentially form a base pair prior to DNA translocation. If this occurs, PP_i release could be stimulated by an allosteric conformational change propagated from the pre-insertion dNTP binding site to the catalytic center ∼30 Å away. Although it could be envisioned that the next nascent base pair would need to swing into the active site; it is possible this base pair could be broken and that another next correct nucleotide could base pair with the next templating base (T_1) after it repositions into the active site.

The Gka-PolC structure, however, shows just a single snapshot of DNA replication, and PP_i release could instead be triggered at any point during the translocation of the next template base into the nascent base pair binding pocket. To visualize this process, we constructed a model of Gka-PolC with the tip of the fingers domain (the index finger) in an open conformation, based on the apo-enzyme structure of *T. aquaticus* DnaE (PDB code 2HPM; (20)). Although the Gka-PolC and Taq-DnaE polymerases share little sequence identity, the structures are highly conserved, with the full enzymes superimposing with an overall RMSD of ∼3 Å and individual domains superimposing with RMSDs ranging from 1.2 to 2.6 Å (16).

With the PolC fingers in an open conformation, as shown in model 2 (Figure 7C), we could readily model a Watson-Crick base pair between the next incoming nucleotide and the next templating base, without having to adjust the position of either the duplex DNA or the PP_i from the previous nucleotide incorporation cycle. In this case, a pre-insertion binding site for both the incoming dNTP and next templating base is created when the fingers open, with positively-charged residues being located in a position where they could contact the tri-phosphate group of the incoming nucleotide in much the same way as they do in the closed ternary complex structure (16). The $PP_i \bullet Mg^{2+}$ generated from the current nucleotide incorporation cycle would need to remain bound to the enzyme in this open conformation, at least until the next base pair starts to form, for this model to account for the kinetic mechanism that we have observed for PolC. For most polymerases, it is thought that dissociation of PP_i accompanies opening of the fingers, but recent structures of the related DNA polymerase β demonstrates that $PP_i \bullet Mg^{2+}$ can remain bound at the active site even when the fingers are open (PDB code 5TB8; (53)). For PolC, we envision that PP_i would be displaced as the β- and γ-phosphate (and associated Mg^{2+}) of the next incoming dNTP (and associated Mg^{2+}) compete for binding to the catalytic aspartates. The dNTP is expected to out-compete PP_i binding because of the additional interactions of the base, ribose, and α-phosphate of the dNTP with the polymerase, templating base, and primer terminus. Thus, in the absence of competition with the next correct nucleotide, release of PP_i would be slow.

In this scenario, PP_i release and translocation of the DNA duplex would both be coupled to the fingers adopting a closed conformation upon binding of the next correct dNTP. Details such as this are difficult to predict, but this translocation mechanism would distinguish the C-family polymerases from other polymerase families. Available crystal structures of A- and B-family DNA polymerases indicate that translocation of the newly formed base pair oc-

curs when the polymerase fingers rotate into an open conformation and conserved tyrosines move to partially occupy the nascent base pair binding pocket (54,55). A stepwise translocation mechanism has been observed for the Y-family translesion DNA polymerase Dpo4, where the primer and template DNA strands translocate separately and involve more subtle conformational changes of the enzyme (56). In contrast, T7 DNA polymerase shows a single translocation step that occurs spontaneously after enzyme opening and concomitant release of pyrophosphate (7).

Implications for the regulation and fidelity of DNA synthesis

The kinetic mechanism that we have defined for PolC can potentially increase DNA replication fidelity in two ways. First, mis-incorporated nucleotides could be removed by pyrophosphorolysis at the polymerase active site if PP_i release is also slow for a mismatch and chemistry is reversible. However, it should be noted that chemistry is already slow for misincorporations in both the forward and reverse directions. Second, formation of a correct Watson-Crick base pair can be sensed at two different stages in the reaction pathway: initially, when the dNTP binds to the $PolC \bullet DNA_{n+1} \bullet PP_i$ complex and again after PP_i has dissociated. This could allow multiple opportunities to select correctly base paired dNTPs over mismatched dNTPs.

Regardless of where the next correct nucleotide binds or the structural basis for the stimulation of PP_i release, this novel mechanism of nucleotide incorporation has profound implications for the regulation of replication in bacteria. Since DNA synthesis cannot continue until PP_i dissociates from the polymerase active site, and because this is stimulated only by binding of the next correct nucleotide, the rate of DNA synthesis catalyzed by PolC can be modulated by the concentration and balance of cellular nucleotide pools. Nucleotide pools have been found to have a profound influence on mutation rates and the rate of the replication fork progression (57–59). Additionally, reversibility of chemistry due to the rate-limiting release of PP_i, would enhance discrimination of incorrectly paired or non-cognate base pairs at the polymerase active site. This has been demonstrated as a mechanism for increasing fidelity by HIV-RT and HCV NS5B (37,47). Moreover, the polymerase could sense DNA damage before committing to replicate the damaged DNA if the damaged base fails to pair with the next incoming nucleotide.

Although the kinetic checkpoint for the next correct dNTP is an intrinsic property of the PolC polymerase active site, it may well be modulated by other factors, such as an active exonuclease active site or other components of the replisome.

Weak DNA binding and the replisome

Another striking feature of PolC is its weak affinity for the DNA substrate, stemming primarily from a fast dissociation of the $PolC \bullet DNA_n$ complex. A similar observation has been reported for *E. coli* Pol IIIα (60), indicating that formation of a low affinity binary complex is a shared characteristic of the bacterial replicative polymerases.

Prolonged interaction between a DNA polymerase and DNA is a pre-requisite for efficient processive DNA synthesis. However, an inherently long-lived $Pol \bullet DNA_n$ complex could be detrimental to cell viability, by reducing both the speed and fidelity of DNA synthesis, as has been observed for a mutant version (E612K) of *E. coli* Pol IIIα (61). Bacterial replication proceeds rapidly, at speeds of up to 1000 nucleotides per second, and a tight binary complex might hinder the translocation of the polymerase along the DNA. During translocation, the existing contacts between the polymerase and the DNA substrate must be broken and reformed as the enzyme moves along the DNA in single base pair steps. Too strong an interaction might result in an energetic barrier to translocation that could slow processive DNA synthesis. Moreover, a $Pol \bullet DNA_n$ complex that is too stable might lead to poor replication fidelity, by preventing efficient partitioning of the DNA between polymerization and proofreading modes after a misincorporation event. For proofreading activity, the DNA substrate poised for extension must dissociate from the polymerization active site of the DNA polymerase and reposition at the exonuclease active site. A tight binary complex, coupled with a fast DNA extension rate, might pose a challenge for efficient switching of the DNA between the polymerization and exonuclease sites.

Nonetheless, if the inherent affinity of PolC for DNA is weak, then how can interactions between PolC and DNA be sustained for the time required for efficient processive synthesis to be achieved? *In vivo,* a DNA polymerase does not function alone. Rather the enzyme is a part of the multi-component replisome where several of the components interact directly with the DNA polymerase and increase its affinity for the DNA. Consistent with this, we found that the β-clamp processivity factor strengthens the affinity of PolC for DNA 4-fold by slowing the dissociation rate of the binary complex 7-fold. Additionally, the N-terminal domain of PolC contains a pair of motifs that are both distantly related to domain V of the DNA polymerase III τ subunit, which could facilitate the interaction between PolC and τ (31,62). This interaction could serve to further enhance binding to DNA as has been documented for the *E. coli* Pol III core (60). The modulation of a polymerase's affinity for its substrates by protein partners might provide additional control over the speed and efficiency of replication in response to cellular conditions.

CONCLUSION AND FUTURE DIRECTIONS

In addition to describing a unique mechanism for processive DNA synthesis, the kinetic pathway that we have defined for *S. aureus* PolC provides a foundation for robust structure-function studies of the C-family bacterial DNA polymerases. Of particular interest are the essential DnaE3 polymerases that are found together with PolC in Gram-positive bacteria and the non-essential DnaE2 polymerases that are found together with essential DnaE1 polymerases in Gram-negative bacteria (63). While many of these polymerases are required for extensive, high-fidelity DNA synthesis, others are responsible for more limited, lower-fidelity DNA synthesis. In *Bacillus subtilis*, DnaE3 is required for initiating DNA synthesis from RNA primers (41) and

DnaE2 from *Mycobacterium tuberculosis* contributes to the emergence of drug resistance (64,65). Further kinetic studies, in conjunction with structure-guided mutagenesis, will be required to elucidate the sources of substrate specificity and accurate vs. error-prone DNA synthesis in the C-family polymerases and to evaluate the potential of these enzymes as therapeutic drug targets.

DATA AVAILABILITY

KinTek Explorer mechanism files are available upon request.

SUPPLEMENTARY DATA

Supplementary Data are available at NAR Online.

ACKNOWLEDGEMENTS

We thank An Li and Shanzhong Gong for assistance in performing preliminary experiments. We thank the following Wadsworth Center core facilities for providing expertise and material support when necessary: media and tissue culture, applied genomic technologies core, biochemistry, and protein expression.

FUNDING

REFERENCES

1. Bebenek,K. and Kunkel,T.A. (2004) Functions of DNA polymerases. *Adv. Protein Chem.*, **69**, 137–165.
2. Steitz,T.A. (1998) A mechanism for all polymerases. *Nature*, **391**, 231–232.
3. Steitz,T.A. (1993) DNA- and RNA-dependent DNA polymerases. *Curr. Opin. Struct. Biol.*, **3**, 31–38.
4. Joyce,C.M. and Benkovic,S.J. (2004) DNA polymerase fidelity: kinetics, structure, and checkpoints. *Biochemistry*, **43**, 14317–14324.
5. Tsai,Y.-C. and Johnson,K.A. (2006) A new paradigm for DNA polymerase specificity. *Biochemistry*, **45**, 9675–9687.
6. Kellinger,M.W. and Johnson,K.A. (2010) Nucleotide-dependent conformational change governs specificity and analog discrimination by HIV reverse transcriptase. *Proc. Natl. Acad. Sci. U.S.A.*, **107**, 7734–7739.
7. Dangerfield,T.L. and Johnson,K.A. (2021) Conformational dynamics during high-fidelity DNA replication and translocation defined using a DNA polymerase with a fluorescent artificial amino acid. *J. Biol. Chem.*, **296**, 100143.
8. Wu,W.J., Yang,W. and Tsai,M.D. (2017) How DNA polymerases catalyse replication and repair with contrasting fidelity. *Nat. Rev. Chem.*, **1**, 0068.
9. Kuchta,R.D., Mizrahi,V., Benkovic,P.A., Johnson,K.A. and Benkovic,S.J. (1987) Kinetic mechanism of DNA polymerase I (Klenow). *Biochemistry*, **26**, 8410–8417.
10. Patel,S.S., Wong,I. and Johnson,K.A. (1991) Pre-steady-state kinetic analysis of processive DNA replication including complete characterization of an exonuclease-deficient mutant. *Biochemistry*, **30**, 511–525.
11. Wong,I., Patel,S.S. and Johnson,K.A. (1991) An induced-fit kinetic mechanism for DNA replication fidelity: direct measurement by single-turnover kinetics. *Biochemistry*, **30**, 526–537.
12. Kunkel,T.A. (2004) DNA replication fidelity. *J. Biol. Chem.*, **279**, 16895–16898.
13. Kool,E.T. (2001) Hydrogen bonding, base stacking, and steric effects in DNA replication. *Annu. Rev. Biophys. Biomol. Struct.*, **30**, 1–22.
14. Joyce,C.M. (1997) Choosing the right sugar: how polymerases select a nucleotide substrate. *Proc. Natl. Acad. Sci.*, **94**, 1619–1622.
15. Donlin,M.J., Patel,S.S. and Johnson,K.A. (1991) Kinetic partitioning between the exonuclease and polymerase sites in DNA error correction. *Biochemistry*, **30**, 538–546.
16. Evans,R.J., Davies,D.R., Bullard,J.M., Christensen,J., Green,L.S., Guiles,J.W., Pata,J.D., Ribble,W.K., Janjic,N. and Jarvis,T.C. (2008) Structure of PolC reveals unique DNA binding and fidelity determinants. *Proc. Natl. Acad. Sci. U.S.A.*, **105**, 20695–20700.
17. Fernandez-Leiro,R., Conrad,J., Scheres,S.H.W. and Lamers,M.H. (2015) cryo-EM structures of the *E. coli* replicative DNA polymerase reveal its dynamic interactions with the DNA sliding clamp, exonuclease and τ. *Elife*, **4**, e11134.
18. Lamers,M.H., Georgescu,R.E., Lee,S.-G., O'Donnell,M. and Kuriyan,J. (2006) Crystal structure of the catalytic α subunit of E. coli replicative DNA polymerase III. *Cell*, **126**, 881–892.
19. Wing,R.A., Bailey,S. and Steitz,T.A. (2008) Insights into the replisome from the structure of a ternary complex of the DNA polymerase III α-subunit. *J. Mol. Biol.*, **382**, 859–869.
20. Bailey,S., Wing,R.A. and Steitz,T.A. (2006) The structure of T. aquaticus DNA polymerase III Is Distinct from eukaryotic replicative DNA polymerases. *Cell*, **126**, 893–904.
21. Baños-Mateos,S., van Roon,A.-M.M., Lang,U.F., Maslen,S.L., Skehel,J.M. and Lamers,M.H. (2017) High-fidelity DNA replication in Mycobacterium tuberculosis relies on a trinuclear zinc center. *Nat. Commun.*, **8**, 855.
22. Leipe,D.D., Aravind,L. and Koonin,E.V. (1999) Did DNA replication evolve twice independently? *Nucleic Acids Res.*, **27**, 3389–3401.
23. Yao,N.Y. and O'Donnell,M.E. (2016) Evolution of replication machines. *Crit. Rev. Biochem. Mol. Biol.*, **51**, 135–149.
24. Yamtich,J. and Sweasy,J.B. (2010) DNA polymerase Family X: function, structure, and cellular roles. *Biochim. Biophys. Acta - Proteins Proteomics*, **1804**, 1136–1150.
25. Lahiri,I., Mukherjee,P. and Pata,J.D. (2013) Kinetic characterization of exonuclease-deficient staphylococcus aureus PolC, a C-family replicative DNA polymerase. *PLoS One*, **8**, e6349.
26. Klemperer,N., Zhang,D., Skangalis,M. and O'Donnell,M. (2000) Cross-utilization of the β sliding clamp by replicative polymerases of evolutionary divergent organisms. *J. Biol. Chem.*, **275**, 26136–26143.
27. Hanes,J.W. and Johnson,K.A. (2008) Real-time measurement of pyrophosphate release kinetics. *Anal. Biochem.*, **372**, 125–127.
28. Johnson,K.A., Simpson,Z.B. and Blom,T. (2009) Global kinetic explorer: a new computer program for dynamic simulation and fitting of kinetic data. *Anal. Biochem.*, **387**, 20–29.
29. Johnson,K.A., Simpson,Z.B. and Blom,T. (2009) FitSpace explorer: an algorithm to evaluate multidimensional parameter space in fitting kinetic data. *Anal. Biochem.*, **387**, 30–41.
30. Kong,X.-P., Onrust,R., O'Donnell,M. and Kuriyan,J. (1992) Three-dimensional structure of the β subunit of E. coli DNA polymerase III holoenzyme: A sliding DNA clamp. *Cell*, **69**, 425–437.
31. Bruck,I. and O'Donnell,M. (2000) The DNA replication machine of a gram-positive organism. *J. Biol. Chem.*, **275**, 28971–28983.

32. Einolf,H.J. and Guengerich,F.P. (2001) Fidelity of nucleotide insertion at 8-oxo-7, 8-dihydroguanine by mammalian DNA polymerase δ. *J. Biol. Chem.*, **276**, 3764–3771.

33. Schlosshauer,M. and Baker,D. (2004) Realistic protein-protein association rates from a simple diffusional model neglecting long-range interactions, free energy barriers, and landscape ruggedness. *Protein Sci.*, **13**, 1660–1669.

34. Joyce,C.M. (2010) Techniques used to study the DNA polymerase reaction pathway. *Biochim. Biophys. Acta - Proteins Proteomics*, **1804**, 1032–1040.

35. Johnson,K.A. (1995) Rapid quench kinetic analysis of polymerases, adenosinetriphosphatases, and enzyme intermediates. *Methods Enzymol.*, **249**, 38–61.

36. Linkuvienė,V., Talibov,V.O., Danielson,U.H. and Matulis,D. (2018) Introduction of intrinsic kinetics of protein–ligand interactions and their implications for drug design. *J. Med. Chem.*, **61**, 2292–2302.

37. Li,A., Gong,S. and Johnson,K.A. (2016) Rate-limiting pyrophosphate release by HIV reverse transcriptase improves fidelity. *J. Biol. Chem.*, **291**, 26554–26565.

38. Li,A., Li,J. and Johnson,K.A. (2016) HIV-1 reverse transcriptase polymerase and RNase H (ribonuclease H) active sites work simultaneously and independently. *J. Biol. Chem.*, **291**, 26566–26585.

39. Mok,M. and Marians,K.J. (1987) The *Escherichia coli* preprimosome and DNA B helicase can form replication forks that move at the same rate. *J. Biol. Chem.*, **262**, 16644–16654.

40. Wang,J.D., Sanders,G.M. and Grossman,A.D. (2007) Nutritional control of elongation of DNA replication by ppGpp. *Cell*, **128**, 865–875.

41. Sanders,G.M., Dallmann,H.G. and McHenry,C.S. (2010) Reconstitution of the B. subtilis replisome with 13 proteins including two distinct replicases. *Mol. Cell*, **37**, 273–281.

42. Raper,A.T., Reed,A.J. and Suo,Z. (2018) Kinetic mechanism of DNA polymerases: contributions of conformational dynamics and a third divalent metal ion. *Chem. Rev.*, **118**, 6000–6025.

43. Kottur,J. and Nair,D.T. (2018) Pyrophosphate hydrolysis is an intrinsic and critical step of the DNA synthesis reaction. *Nucleic Acids Res.*, **46**, 5875–5885.

44. Weaver,T.M., Cortez,L.M., Khoang,T.H., Washington,M.T., Agarwal,P.K. and Freudenthal,B.D. (2020) Visualizing Rev1 catalyze protein-template DNA synthesis. *Proc. Natl. Acad. Sci. U.S.A.*, **117**, 25494–25504.

45. Hanes,J.W. and Johnson,K.A. (2007) A novel mechanism of selectivity against AZT by the human mitochondrial DNA polymerase. *Nucleic Acids Res.*, **35**, 6973–6983.

46. Hanes,J.W., Thal,D.M. and Johnson,K.A. (2006) Incorporation and replication of 8-oxo-deoxyguanosine by the human mitochondrial DNA polymerase. *J. Biol. Chem.*, **281**, 36241–36248.

47. Villalba,B. and Johnson,K.A. (2020) Rate-limiting pyrophosphate release by hepatitis C virus polymerase NS5B improves fidelity. *J. Biol. Chem.*, **295**, 16436–16444.

48. Dieckman,L.M., Johnson,R.E., Prakash,S. and Washington,M.T. (2010) Pre-steady state kinetic studies of the fidelity of nucleotide incorporation by yeast DNA polymerase δ. *Biochemistry*, **49**, 7344–7350.

49. Johnson,R.S., Strausbauch,M., Cooper,R. and Register,J.K. (2008) Rapid kinetic analysis of transcription elongation by escherichia coli RNA polymerase. *J. Mol. Biol.*, **381**, 1106–1113.

50. Johnson,R.S., Strausbauch,M. and Carraway,J.K. (2011) Rapid pyrophosphate release from transcriptional elongation complexes appears to be coupled to a nucleotide-induced conformational change in *E. coli* core polymerase. *J. Mol. Biol.*, **412**, 849–861.

51. Foster,J.E., Holmes,S.F. and Erie,D.A. (2001) Allosteric binding of nucleoside triphosphates to RNA polymerase regulates transcription elongation. *Cell*, **106**, 243–252.

52. Kennedy,S.R. and Erie,D.A. (2011) Templated nucleoside triphosphate binding to a noncatalytic site on RNA polymerase regulates transcription. *Proc. Natl. Acad. Sci. U.S.A.*, **108**, 6079–6084.

53. Reed,A.J., Vyas,R., Raper,A.T. and Suo,Z. (2017) Structural insights into the post-chemistry steps of nucleotide incorporation catalyzed by a DNA polymerase. *J. Am. Chem. Soc.*, **139**, 465–471.

54. Berman,A.J., Kamtekar,S., Goodman,J.L., Lázaro,J.M., De Vega,M., Blanco,L., Salas,M. and Steitz,T.A. (2007) Structures of phi29 DNA polymerase complexed with substrate: The mechanism of translocation in B-family polymerases. *EMBO J.*, **26**, 3494–3505.

55. Johnson,S.J., Taylor,J.S. and Beese,L.S. (2003) Processive DNA synthesis observed in a polymerase crystal suggests a mechanism for the prevention of frameshift mutations. *Proc. Natl. Acad. Sci. U.S.A.*, **100**, 3895–3900.

56. Rechkoblit,O., Malinina,L., Cheng,Y., Kuryavyi,V., Broyde,S., Geacintov,N.E. and Patel,D.J. (2006) Stepwise translocation of Dpo4 polymerase during error-free bypass of an oxoG lesion. *PLoS Biol.*, **4**, e11.

57. Gon,S., Napolitano,R., Rocha,W., Coulon,S. and Fuchs,R.P. (2011) Increase in dNTP pool size during the DNA damage response plays a key role in spontaneous and induced-mutagenesis in *Escherichia coli*. *Proc. Natl. Acad. Sci. U.S.A.*, **108**, 19311–19316.

58. Yao,N.Y., Schroeder,J.W., Yurieva,O., Simmons,L.A. and O'Donnell,M.E. (2013) Cost of rNTP/dNTP pool imbalance at the replication fork. *Proc. Natl. Acad. Sci. U.S.A.*, **110**, 12942–12947.

59. Laureti,L., Selva,M., Dairou,J. and Matic,I. (2013) Reduction of dNTP levels enhances DNA replication fidelity in vivo. *DNA Repair (Amst.)*, **12**, 300–305.

60. Georgescu,R.E., Kurth,I., Yao,N.Y., Stewart,J., Yurieva,O. and O'Donnell,M. (2009) Mechanism of polymerase collision release from sliding clamps on the lagging strand. *EMBO J.*, **28**, 2981–2991.

61. Maki,H., Mo,J.Y. and Sekiguchi,M. (1991) A strong mutator effect caused by an amino acid change in the alpha subunit of DNA polymerase III of Escherichia coli. *J. Biol. Chem.*, **266**, 5055–5061.

62. Timinskas,K. and Venclovas,Č. (2011) The N-terminal region of the bacterial DNA polymerase PolC features a pair of domains, both distantly related to domain V of the DNA polymerase III τ subunit. *FEBS J.*, **278**, 3109–3118.

63. Timinskas,K., Balvočiūtė,M., Timinskas,A. and Venclovas,Č. (2014) Comprehensive analysis of DNA polymerase III α subunits and their homologs in bacterial genomes. *Nucleic Acids Res.*, **42**, 1393–1413.

64. Boshoff,H.I.M., Reed,M.B., Barry,C.E. and Mizrahi,V. (2003) DnaE2 polymerase contributes to in vivo survival and the emergence of drug resistance in Mycobacterium tuberculosis. *Cell*, **113**, 183–193.

65. Warner,D.F., Ndwandwe,D.E., Abrahams,G.L., Kana,B.D., Machowski,E.E., Venclovas,Č. and Mizrahi,V. (2010) Essential roles for imuA′- and imuB-encoded accessory factors in DnaE2-dependent mutagenesis in *Mycobacterium tuberculosis*. *Proc. Natl. Acad. Sci. U.S.A.*, **107**, 13093–13098.